1 INTRODUCTION

The reliability and performance of modern pumps is often limited by shaft vibrations. These vibrations are strongly influenced by the hydrodynamic forces induced by the laminar or turbulent fluid flow in narrow annular gaps. In general, the annular gap flow is three dimensional: the circumferential flow driven by viscous forces is superimposed by a pressure driven axial flow. In addition, this axial flow convects swirl into the annular gap. So far, there is a severe lack of understanding this flow. I.e. the state of the art simulation methods fail in reliably predicting the induced fluid forces.

Within modern pumps two essential machine elements exist, exerting hydrodynamic forces on the rotating shaft: (i) contactless annular seals and (ii) media lubricated journal bearings, c.f. Figure 1 (pressure $\tilde{p}$, volume flow $\tilde{Q}$, rotational frequency $\tilde{\Omega}$).

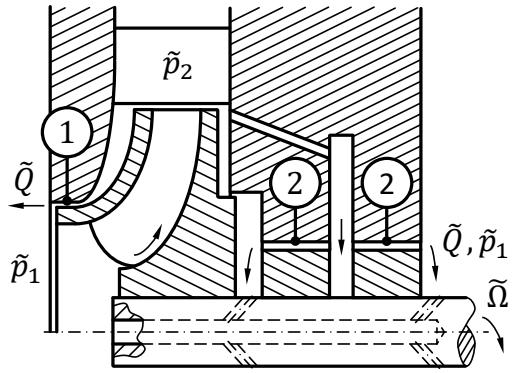

Figure 1. Schematic diagram of a centrifugal pump, c.f. [1]: (1) annular seal; (2) media lubricated journal bearing.

Both machine elements, the annular seal and the journal bearing consist of a comparable geometry, a liquid-filled narrow annulus with a mean clearance $\tilde{\bar{h}} := \tilde{R}_{\mathrm{out}} - \tilde{R}$ (outer radius $\tilde{R}_{\mathrm{out}}$, shaft radius $\tilde{R}$) and an inner shaft rotating at a constant rotational frequency $\tilde{\Omega}$. The main task of the annular seal is to separate zones of different pressure $\tilde{p}_2 > \tilde{p}_1$ at a lowest possible leakage $\tilde{Q}$, whereas the media lubricated journal bearing partly carries the weight of the shaft and the load of the turbomachine. In addition, the journal bearing uses the primary process medium as a lubricant and the available pressure difference $\Delta\tilde{p} = \tilde{p}_2 - \tilde{p}_1$ ($\tilde{p}_2 > \tilde{p}_1$) within the pump for supply purpose.

Besides the differentiation by function, a further separation of annular seals and journal bearings is in achieved by analysing the existing flow phenomena, respectively the influence of fluid inertia within the annulus. To distinguish whether or not inertia has to be taken into account, a characteristic parameter ψRe_φ (relative clearances $\psi := \tilde{\bar{h}}/\tilde{R}$, Reynolds number $Re_\varphi := \tilde{\Omega}\tilde{R}\tilde{\bar{h}}/\tilde{\nu}$) is used [1–3]. This modified Reynolds number characterizes the influence of inertia effects in relation to viscous forces and distinguishes three different ranges: If (i) $\psi Re_\varphi \ll 1$ fluid inertial is negligible in relation to viscous forces; (ii) $\psi Re_\varphi \approx 1$ convective terms need to be considered within the calculation and (iii) $\psi Re_\varphi \gg 1$ fluid inertia is dominant in relation to viscous forces.

Initially concentrating on the annular seal, the typical geometrical and operating conditions like shaft diameter $\tilde{D} := 2\tilde{R} \sim 0.1\,\mathrm{m}$, relative clearance $\psi \sim 10\,‰$, rotation frequency $\tilde{\Omega} \sim 10^2\,1/s$ and Reynolds number $Re_\varphi = 10^3 \ldots 10^5$ result in the characteristic parameter $\psi Re_\varphi \sim 10^1 \ldots 10^3 \gg 1$. This indicates, that the flow within an annular seal is dominated by inertial effect. To further distinguish between laminar and turbulent flow the critical Reynolds number $Re_{\mathrm{CRIT}} := 41.3\sqrt{1/\psi} \sim 10^2$ is used. If this limit is exceeded, the previously purely laminar flow in the lubrication gap is increasingly disturbed by turbulent flow phenomena. In case of modern annular seals, the describing Reynolds numbers are always larger than the critical Reynolds number indicating fully turbulent flow within the annulus.

In the case of classic journal bearings the typical geometrical and operating conditions like shaft diameter $\tilde{D} := 2\tilde{R} \sim 0.1\,\mathrm{m}$, relative clearances $\psi \sim 1\,‰$, rotation frequency $\tilde{\Omega} \sim 10^2\,1/s$ and Reynolds number $Re_\varphi = 10^0 \ldots 10^1$ result in the characteristic parameter $\psi Re_\varphi \sim 10^{-2} \ldots 10^{-1} \ll 1$. This indicates, that the flow within a classic journal bearing is dominated by viscous effects. The describing Reynolds number is always smaller than the critical Reynolds number $Re_{\mathrm{CRIT}} \sim 10^3$ indicating laminar flow within the bearing.

However, for media lubricated journal bearings such an asymptotical distinction between seal or bearing is not possible. Due to the lower viscosity of the lubricant as well as larger shaft diameters, larger relative clearances and significant axial pressure differences across the bearing the characteristic parameter is of the order of magnitude $\psi Re_\varphi \sim 1$, resulting in a need of considering convective terms within the calculation. In addition, the Reynolds number varies within a range of $Re_\varphi < Re_{\mathrm{CRIT}} < Re_\varphi$, indicating both laminar and turbulent flow depending on the operation point as well as the describing geometry. These reasons indicate a continuous transition between bearing and annular seal. Table 1 gives a brief overview of the typical geometry and

operating conditions of media lubricated journal bearings and annular seals.

Table 1. Typical geometry and operating conditions of media lubricated journal bearings and annular seals.

bearing clearance $\tilde{\bar{h}}$	$10 \dots 240$ mm
relative bearing clearance $\psi \coloneqq \tilde{\bar{h}}/\tilde{R}$	$1 \dots 10$ ‰
rotating frequency $\tilde{\Omega}$	$1000 \dots 3600$ rpm
relative eccentricity ε	$0 \dots 1$
pressure drop across the annulus	$0 \dots 20$ bar
lubrication fluid	water, etc.
Reynolds number	$20 \dots 10^5$
critical Reynolds number	$400 \dots 1300$

Like the theoretical considerations of annular seals and journal bearings, the existing literature also focuses to a large extent on the asymptotic boundary cases, c.f. [4–8]. Annular seals are in general treated using the Bulk-Flow-Model (BFM) based on the work of Childs [4]. Within the BFM, mass and momentum conservation equations are solved and shear stresses within the fluid are neglected due $\psi Re_\varphi \gg 1$ assuming constant velocity profiles.

Journal bearings with weather laminar or turbulent flow are usually treated by Reynolds differential equation (RDE) of hydrodynamic lubrication theory [9]. In the laminar flow case ($\psi Re_\varphi \ll 1$) convective terms are neglected. For turbulent flow ($\psi Re_\varphi \gtrsim 1$) convective terms are still neglected and the inertia effects, e.g. turbulence effects, are modeled by adding empirical correction coefficients depending on the respective operating point [6]. This asymptotic view, with a few exceptions (San Andrés [10], Arghir [11]), leads to a large knowledge gap in the field of media lubricated journal bearings. In addition, publications dealing with this kind of machine element and containing both calculation results and experimental investigations of one single author are limited. Furthermore, in the majority of publications, the fundamental measurement uncertainties and their effect on the experimental results are only insufficiently considered.

To fill this knowledge gap, on the experimental as well as the calculation side, two similar test rigs are designed, build, and operated at the TU Darmstadt. The generic experiments cover the relevant parameter range for turbulent and laminar flow in pumps. The calculations are carried out using the TU Darmstadt simulation method CAPM [1].

2 THE TU DARMSTADT SIMULATION METHOD (CAPM)

Based on the work of Lang [1] the Clearance Averaged Pressure Model (CAPM) describes a generic annular gap flow, c.f. Figure 2.

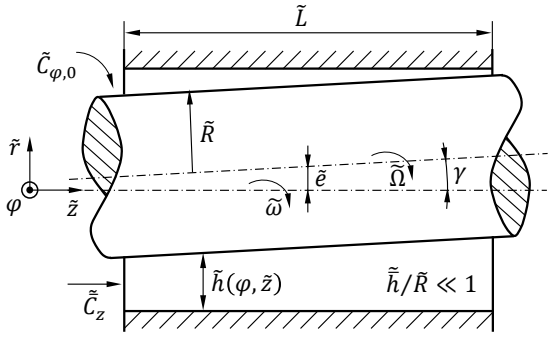

Figure 2. Generic annular gap flow [3].

The flow inside the annulus is fully described by 8 dimensionless parameters: the pressure distribution inside the annulus p, the modified Reynolds number $\psi Re_\varphi^{n_f}$ with the Hirs exponent n_f, the flow number ϕ, the preswirl $C_{\varphi 0}$, the dimensionless length L, the relative eccentricity ε, the misalignment angle γ and the dimensionless orbit frequency ω.

$$p = p(\psi Re_\varphi^{n_f}, \phi, C_{\varphi 0}, L, \varepsilon, \gamma, \omega) \text{ with}$$
$$p \coloneqq \frac{2\tilde{p}}{\tilde{\varrho}\tilde{\Omega}^2\tilde{R}^2}, \phi \coloneqq \frac{\tilde{\bar{C}}_z}{\tilde{\Omega}\tilde{R}}, C_{\varphi 0} \coloneqq \frac{\tilde{C}_{\varphi 0}}{\tilde{\Omega}\tilde{R}}, \quad (1)$$
$$L = \frac{\tilde{L}}{\tilde{R}}, \varepsilon \coloneqq \frac{\tilde{e}}{\tilde{\bar{h}}}, \omega = \frac{\tilde{\omega}}{\tilde{\Omega}}.$$

The CAPM formulates the following dimensionless conservation equations for mass, circumferential and axial momentum:

$$\frac{\partial}{\partial\varphi} h \int_0^1 w_\varphi \, dy + \frac{\phi}{L}\frac{\partial}{\partial z} h \int_0^1 c_z \, dy = 0, \quad (2)$$

$$\frac{\partial}{\partial\varphi} h \int_0^1 w_\varphi^2 \, dy + \frac{\phi}{L}\frac{\partial}{\partial z} h \int_0^1 w_\varphi c_z \, dy = -\frac{h}{2}\frac{\partial p}{\partial\varphi} + \frac{\tau_{Stat,\varphi} - \tau_{Rot,\varphi}}{2\psi}, \quad (3)$$

$$\phi \frac{\partial}{\partial\varphi} h \int_0^1 w_\varphi c_z \, dy + \frac{\phi^2}{L}\frac{\partial}{\partial z} h \int_0^1 c_z^2 \, dy = -\frac{h}{2L}\frac{\partial p}{\partial z} + \frac{\tau_{Stat,z} - \tau_{Rot,z}}{2\psi}. \quad (4)$$

The wall shear stresses τ_{Stat}, τ_{Rot} are modeled using Hirs' approach [1, 3, 12] by means of the Fanning friction factor f as $\tilde{\tau}_{Wall} = f\tilde{\varrho}\tilde{C}_{ref}^2/2$

(reference relative velocity $\tilde{C}_{ref}$, density $\tilde{\varrho}$). The velocity profiles for circumferential w_φ and axial velocity c_z are treated using exponential ansatz functions, c.f. [6, 13]. The corresponding equation system is then solved numerically using an iterative SIMPLEC algorithm. For further information on the describing equations and the used algorithm, refer to the work of Lang [1] and Robrecht [14].

3 EXPERIMENTAL SETUP

The experimental investigations, are carried out by two worldwide unique test rigs. To achieve similitude, both test rigs are designed with a geometric similarity in their main dimensions. Each test bench uses two magnetic bearings to (i) support the rotor as well as an inherent (ii) force and (iii) displacement measurement system. The different rotor diameters of the test rigs allow an investigation of the characteristic parameter ψRe_φ in the range of $1 < \psi Re_\varphi < 100$ for the larger, turbulent test rig and $\psi Re_\varphi \leq 1$ for the smaller, laminar test rig. Figure 3 shows the TU Darmstadt annular gap flow test field with the turbulent test rig in the front and the laminar test rig behind. The magnetic bearings for the turbulent test rig were intentionally used by Knopf [15] whereas the magnetic bearings of the laminar test rig are the same as those used by Baumann [16].

The following concentrate on the detailed design of the test benches as well as the associated performance data and measurement uncertainties. For the sake of simplicity, the main components of the test rigs are explained by means of the turbulent test rig.

3.1 Turbulent Test Rig

As illustrated in Figure 4 the turbulent test rig consists of the following 5 components: (i) two active magnetic bearings (AMB) supporting the rotor; (ii) the inlet; (iii) the gap module; (iv) the outlet and (v) two mechanical seals to seal the test rig against the surrounding area.

At first the used magnetic bearings are considered. Compared to conventional bearings such as ball or journal bearings used by several authors [4, 6, 10, 11], magnetic bearings have the advantage of a completely contactless and thus frictionless support of the rotor. In addition, using AMBs has the advantage of an inherent force and displacement measuring system as well as the ability to displace and excite the shaft at user defined frequencies. Due to these advantages, the use of active magnetic bearings is ideal for determining the static and dynamic characteristics of annular gap flows.

To measure the induced hydrodynamic forces within the annulus, the AMBs of the turbulent test rig are equipped with 8 hall sensors each, measuring the magnetic flux density $\tilde{B}$ with in the air gap between rotor and stator. The corresponding force of each pole $\tilde{F}_{H,i}$ (pole surface $\tilde{A}$, magnetic field constant $\tilde{\mu}_0$) yields,

$$\tilde{F}_{H,i} = \frac{\tilde{A}}{2\tilde{\mu}_0}\tilde{B}_i^2, \quad (i = 1..8). \tag{5}$$

Due to the dependence of the magnetic flux density on the position of the rotor within the magnetic bearing, the hall sensors have to be calibrated. This

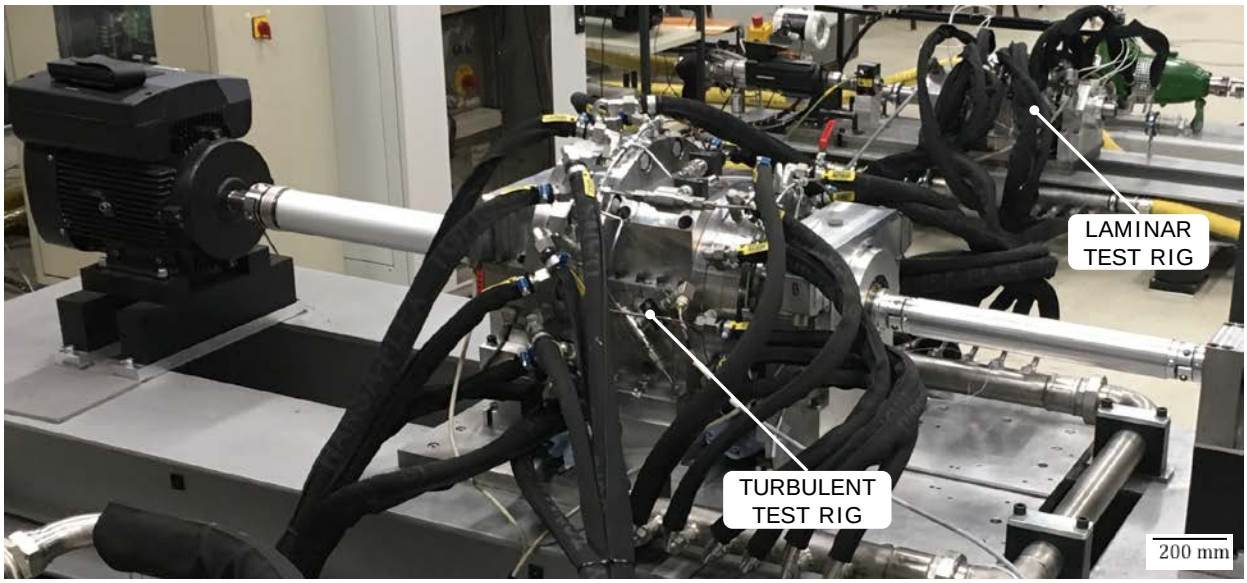

Figure 3. The TU Darmstadt annular gap flow test field.

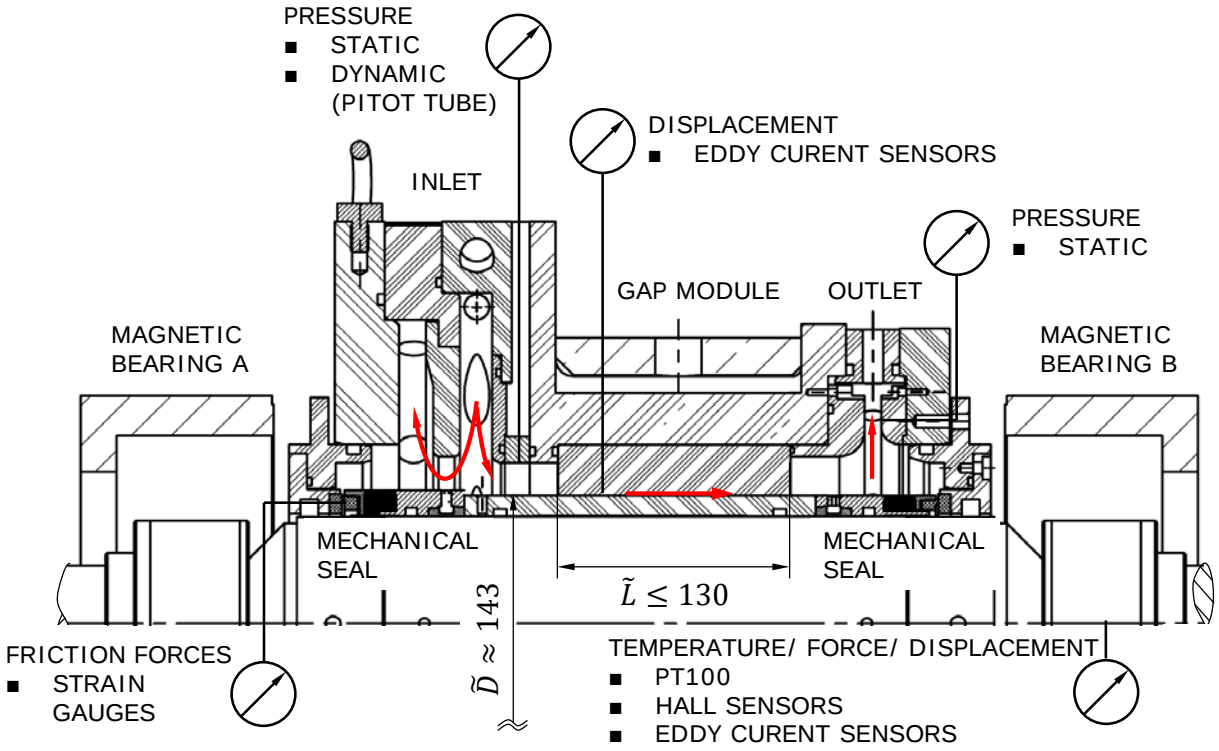

Figure 4. Main components and measurement parameters of the turbulent test rig.

is done using a modified iterative process initially developed by Krüger [17]. The calibration is carried out using the known rotor mass and its center of gravity as a reference force $\tilde{F}_{\mathrm{ref}}$. With an unloaded shaft, the force measurement of the magnetic bearing with an eccentrically positioned rotor in the AMB must output the mass as well as the centre of gravity of the rotor. Figure 5 shows an example of the force measurement uncertainty $\delta_{\mathrm{F,hall}} := \tilde{F}/\tilde{F}_{\mathrm{ref}} - 1$ before and after the position-dependent calibration.

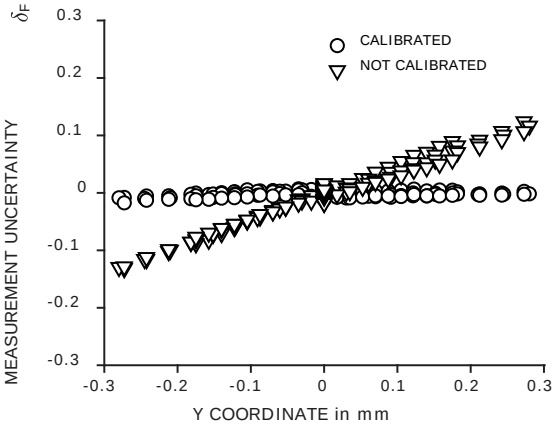

Figure 5. Calibrated force measurement.

The measurement uncertainty after calibration reduces to $\tilde{\delta}_{\mathrm{F,hall}} \pm 0.035\tilde{F}$. The displacement of the rotor inside the AMB is measured using 4 eddy current sensors with an uncertainty of $\tilde{\delta}_{\mathrm{pos}} \leq 6\ \mu\mathrm{m}$. To monitor the temperature of each AMB, each is equipped with two PT100 temperature sensors. Table 2 gives additional information on the magnetic bearing.

Table 2. Properties of the magnetic bearing [17].

manufacturer	MECOS AG
resting gap	1.3 mm
pole width	18 mm
pole length	48 mm
number of windings per pole pair	306
bias current	4 A
maximum force per axis	890 N

The inlet is specially designed to generate swirled flows in front of the annulus. As it is knows form eqn. (1) the pressure field inside the annulus is influenced by the preswirl $C_{\varphi 0}$ right before the gap. For targeted investigation and quantification of the influence on the pressure field, the fluid is injected tangentially into the inlet. By dividing the flow into two parts, gap and bypass volume flow, it is possible to vary the circumferential velocity component in front of the annulus continuously, c.f. Figure 6. To measure the circumferential velocity component before entering the gap, a pitot tube is used. Both test rigs are capable of generating a preswirl in the range of $C_{\varphi 0} = 0 \ldots 1.4$.

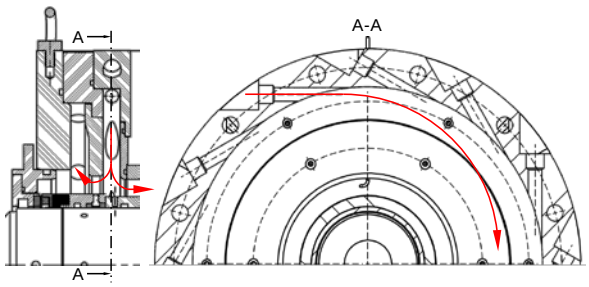

Figure 6. Cross section of the inlet.

In order to determine the position of the rotor within the gap module, the position of the shaft is measured at 2 planes: (i) at the entrance and (ii) exit of the lubrication gap. This is done by using two eddy current sensors (90° arrangement) with an absolute uncertainty of $\tilde{\delta}_{\mathrm{pos}} \leq 1.5\,\mu\mathrm{m}$. The supply pressure is measured at the inlet of the gap module by using 4 wall pressure taps equally space around annulus ($\tilde{\delta}_{\mathrm{P0}} \leq 0.02\,\mathrm{bar}$). The pressure difference across the annulus is measured by a differential pressure sensor with an absolute uncertainty of $\tilde{\delta}_{\mathrm{dp}} \leq 0.1\,\mathrm{bar}$. The turbulent test rig is designed for pressure differences of up to 20 bar.

To seal the test rig against the environment, the fluid path is sealed with two mechanical seals. These allow rotation of the shaft as well as other relative movements with respect to the stator, e.g. dynamic excitations to identify the dynamic characteristics of the annular gap flow. However, during the excitation, force measurement uncertainties occur at the seals due to friction. In order to measure these forces and to reduce the overall uncertainty, four strain gauges are distributed in circumferential direction on the counter ring of the mechanical seal. With these strain gauges, calibrated on a specially designed rig, the resulting friction forces can be determined up to $\tilde{\delta}_{\mathrm{fric}} = \pm 14\,\mathrm{N}$. Table 3 gives additional information on the test rig.

Table 3. Properties of the turbulent test rig.

relative bearing clearance ψ	1…10 ‰
dimensionless length L	0.3…1.83
relative eccentricity ε	0…0.93
preswirl $C_{\varphi 0}$	0…1.4
flow number ϕ	0…6
pressure drop across the annulus $\Delta\tilde{p}$	0…20 bar
maximum supply pressure $\tilde{p}_0$	50 bar
maximum rotational frequency $\tilde{\Omega}$	2000 1/min
lubricant	water
annulus material	stainless steel 1.4301

3.2 Laminar Test Rig

As stated above, the laminar test rig is designed to cover characteristic parameters $\psi Re_{\varphi} \leq 1$. It also consists of the 5 components: (i) two active magnetic bearings (AMB) supporting the rotor; (ii) the inlet; (iii) the gap module; (iv) the outlet and (v) two mechanical seals to seal the test rig against the surrounding area. In comparison to the magnetic bearings of the turbulent test rig, the force of the magnetic bearings of the laminar test rig is not determined by the use of hall sensors, but by the means of the force-current-position characteristic of each magnetic bearing, c.f. Figure 7. By measuring the position of the rotor in the magnetic bearing as well as the used control current during operation, the force generated by the bearing is given by Figure 7.

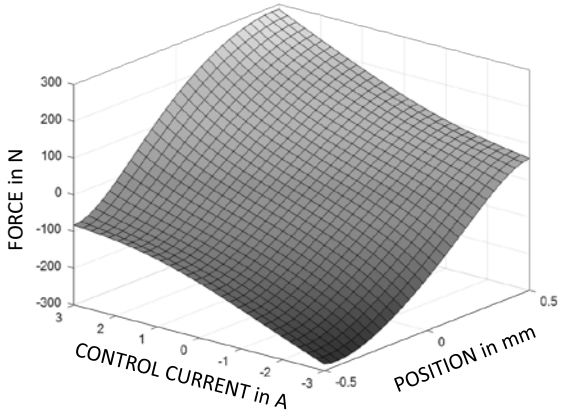

Figure 7. Magnetic bearing characteristics.

Table 4 and Table 5 give additional information on the magnetic bearing as well as the laminar test rig.

Table 4. Properties of the magnetic bearing [16].

manufacturer	TU DARMSTADT
resting gap	1.3 mm
pole width	11 mm
pole length	26 mm
number of windings per pole pair	208
bias current	3 A
maximum force per axis	200 N

Table 5. Properties of the laminar test rig.

relative bearing clearance ψ	1…10 ‰
dimensionless length L	1 …3.13
relative eccentricity ε	0…0.93
preswirl $C_{\varphi 0}$	0…1.4
flow number ϕ	0…6
pressure drop across the annulus $\Delta\tilde{p}$	0…5 bar
maximum supply pressure $\tilde{p}_0$	20 bar
maximum rotational frequency $\tilde{\Omega}$	3600 1/min
lubricant	water
annulus material	stainless steel 1.4301

4 RESULTS

In the following, measurement as well as calculation results for turbulent media lubricated journal bearings are presented. The dimensionless load carrying capacity as a function of relative eccentricity at different Reynolds numbers without axial flow is investigated. Subsequently, the effect of an axial flow component in journal bearings on the load capacity is examined. Finally, the measurement results are compared to different calculation methods (CFD, RDE, CAPM). The results based on the turbulent Reynolds differential equation were obtained in cooperation with the Chair of Machine Elements and Tribology at the Otto von Guericke University Magdeburg.

Figure 8 displays the influence of different Reynolds numbers on the dimensionless load $F := 2\tilde{F} / (\tilde{\varrho}\tilde{\Omega}^2\tilde{R}^2\tilde{R}\tilde{L})$, density $\tilde{\varrho}$, of a turbulent media lubricated journal bearing with no axial flow $\phi = 0$ at increasing eccentricity. The markers represent the experimental results, whereas the solid lines represent the calculation results using Reynolds equation.

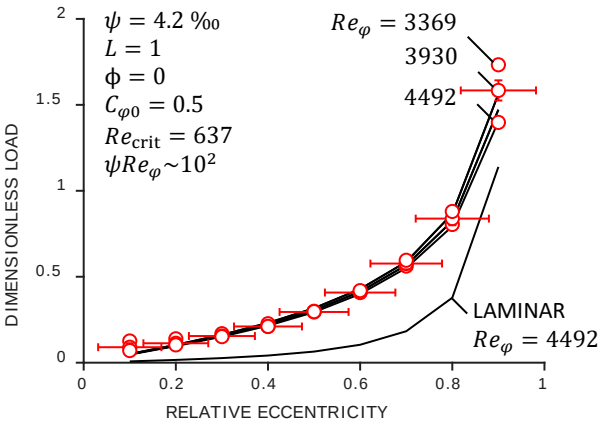

Figure 8. Dimensionless load of a turbulent media lubricated journal bearing without axial flow (marker: experiment, solid line: prediction using RDE).

As expected the dimensionless load increases with increasing eccentricity and decreases with increasing Reynolds number. The predictions based on a modified turbulent Reynolds equation show a good agreement between calculation and measurement. When calculating the turbulent gap flow, based on the standard Reynolds equation for oil lubricated bearing, however, large differences in the dimensionless load are observed. The load capacity of the journal bearing is clearly underestimated over the entire eccentricity range. This is due to the neglect of the inertia terms on the left hand side of momentum equations during derivation of the RDE. As intentionally stated, neglecting inertia terms is only valid in ranges $\psi Re_\varphi \ll 1$. However, the characteristic parameter of the investigated flow is of order of magnitude $\psi Re_\varphi \sim 10^2$, meaning that the neglect is unreasonable and convective terms have to be taken into account.

In modern pumps media lubricated journal bearings are supplied by an axial pressure gradient. The influence on the load capacity is shown in Figure 9.

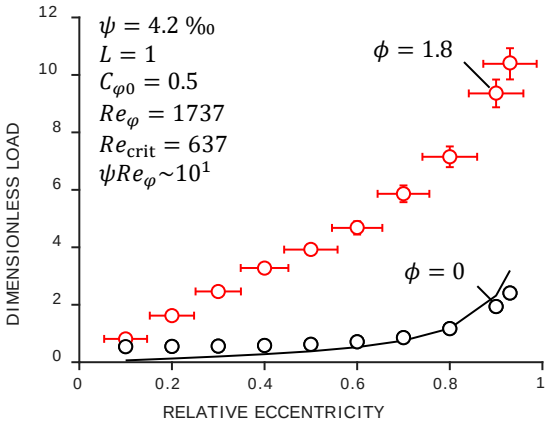

Figure 9. Influence of the axial flow on the dimensionless load (marker: experiment, solid line: prediction using RDE).

In the presence of an axial pressure gradient across the annulus, the flow is superimposed by a significant axial velocity component $\phi \neq 0$, resulting in a substantially increase of load capacity over the whole eccentricity range. The formerly good agreement in the calculation of turbulent journal bearings by means of the modified Reynolds equation vanish. This is due to the formation of an inertia driven centering force at eccentric shaft position and presence of an axial pressure gradient, the Lomakin effect [18]. The occurrence of this effect, typical for the operation of turbulent annular seals, supports the hypothesis of a continuous transition between plain journal bearings and turbulent annular seals.

Considering the significant differences in predicting the characteristics of turbulent media lubricated journal bearings with an axial flow component, the need for an improved reliable and efficient approach arises. Figure 10 compares the measurement results to calculations based on the modified turbulent Reynolds equation as well as the results obtained by the TU Darmstadt simulation method CAPM.

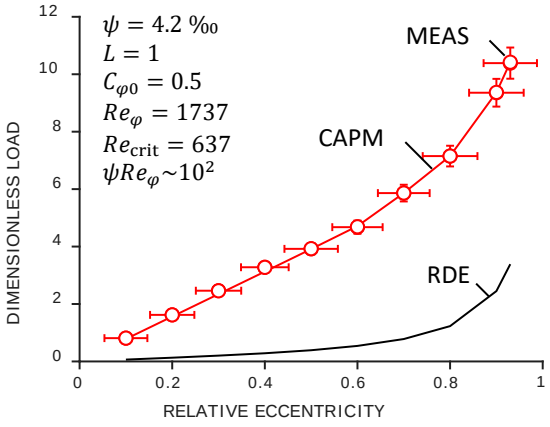

Figure 10. Dimensionless load of a turbulent media lubricated journal bearing with axial flow.

In the presence of an axial pressure gradient, the TU Darmstadt simulation method CAPM is superior to the modified turbulent Reynolds equation. The increase of load capacity due to the Lomakin effect is well predicted over the entire eccentricity range. Furthermore, there is a very good agreement between the measurement results and the simulation method CAPM.

5 CONCLUSIONS

With media lubricated journal bearings, a machine element exists in modern pumps, which represents a continuous transition between classic journal bearings dominated by viscous forces and annular seals dominated by inertia effect. The influence of these components on harmful shaft vibrations is only marginally understood. Furthermore, state of the art calculation methods such as modified Reynolds equations fail to predict the characteristics. To fill this knowledge gap two similar test rigs are operated at the TU Darmstadt. The generic experiments cover the relevant parameter range for turbulent and laminar flow in pumps. The measurement results, with focus on turbulent flows, underline hypotheses of the serious inadequacies in the design of such components by the established methods. This becomes particularly clear in the presence of an axial pressure gradient and the associated formation of the Lomakin effect due to an eccentric shaft position. Due to the neglect of convective terms, the load capacity of media lubricated plain bearings is significantly underestimated by state of the art simulation methods. These inadequacies can be compensated by targeted modelling of the gap flow on the basis of solving of mass and momentum equations.

6 ACKNOWLEDGEMENTS

The presented results were obtained within the research project “Fördermediengeschmierte Gleitlager in Pumpen”, project No. 19225 BG/2, funded by the program for promoting the Industrial Collective Research (IGF) of the German Ministry of Economic Affairs and Energy (BMWi), approved by the Arbeitsgemeinschaft industrieller Forschungsvereinigungen “Otto von Guericke” e.V. (AiF). We want to thank all the participants of the working group as well as the Chair of Machine Elements and Tribology at the Otto von Guericke University Magdeburg for the constructive and close collaboration.

7 REFERENCES

1. Lang, S.: Effiziente Berechnung von Gleitlagern und Dichtspalten in Turbomaschinen von Sebastian Roland Lang. Dissertation, Technische Universität Darmstadt, 2017. Shaker Verlag, Aachen (2018)
2. Kahlert, W.: Der Einfluß der Trägheitskräfte bei der hydrodynamischen Schmiermitteltheorie. Ing. arch (1948). https://doi.org/10.1007/BF00534497
3. Lang, S., Pelz, P.F.: Unified Prediction of Hydrodynamic Forces in Plain Annular Seals and Journal Bearings by means of an Analytically Derived Design Tool. 3rd International Rotating Equipment Conference (IREC) Pumps, Compressors and Vacuum Technology 2016, Duesseldorf, Germany (2016)
4. Childs, D.W.: Turbomachinery rotordynamics. Phenomena, modeling, and analysis. Wiley, New York (1993)
5. Blumenthal, H.e.a.: Experimentelle Untersuchung hydrodynamischer Radialgleitlager mit Wasserschmierung, Kompendium 49 Tribologie-Fachtagung, Göttingen, Band II, (2008)
6. Constantinescu, V.N., Galetuse, S.: Operating Characteristics of Journal Bearings in Turbulent Inertial Flow. J. Lub. Tech. (1982). https://doi.org/10.1115/1.3253177
7. Illner, T., Bartel, D., Deters, L.: Determination of the transition speed in journal bearings

under consideration of bearing deformation. Tribology International **82**, 58–67 (2015)

8. Pfeiffer, P., Schwarze, H.: Experimentelle Untersuchung hydrodynamischer Radialgleitlager mit Wasserschmierung Experimental study of hydrodynamic radial bearings with water lubrication. Wasserkraft mehr Wirkungsgrad+ mehr Ökologie= mehr Zukunft(45), 219–226 (2011)
9. REYNOLDS, O.: On the Theory of Lubrication and Its Application to Mr. Beauchamp Tower's Experiments, Including an Experimental Determination of the Viscosity of Olive Oil. Phil. Trans. Roy. Soc. **1**, 157 (1885)
10. Andrés, L.S., Soulas, T., Fayolle, P.: A Bulk-Flow Model of Angled Injection Lomakin Bearings. J. Eng. Gas Turbines Power (2007). https://doi.org/10.1115/1.2227032
11. Arghir, M., Hélène, M., Frene, J.: Analysis of Tangential-Against-Rotation Injection Lomakin Bearings. J. Eng. Gas Turbines Power (2005). https://doi.org/10.1115/1.1924632
12. Hirs, G.G.: A systematic study of turbulent film flow. J. Lub. Tech. **96**(1), 118–126 (1974)
13. King, K.F., Taylor, C.M.: An Estimation of the Effect of Fluid Inertia on the Performance of the Plane Inclined Slider Thrust Bearing With Particular Regard to Turbulent Lubrication. J. Lub. Tech. (1977). https://doi.org/10.1115/1.3452961
14. Robrecht, R.M., Kuhr, M.M.G., Pelz, P.F.: CAPM vs. Bulk Flow Model and Reynolds equation – reliable and efficient prediction of force and leakage for annular gaps in pumps. 4rd International Rotating Equipment Conference (IREC) Pumps, Compressors and Vacuum Technology 2016, Duesseldorf, Germany (2019)
15. Knopf, E.: Identifikation der Dynamik turbulenter Gleitlager mit aktiven Magnetlagern. Zugl.: Darmstadt, Techn. Univ., Diss., 2001. Forschungsberichte Mechatronik & Maschinenakustik. Shaker, Aachen (2001)
16. Baumann, K.: Dynamische Eigenschaften von Gleitlagern in An- und Auslaufvorgängen. Zugl.: Darmstadt, Techn. Univ., Diss., 2010. Berichte aus dem Maschinenbau. Shaker, Aachen (2011)
17. Krüger, T.: Experimentelle Untersuchung von Quetschfilmdämpfern mit Hilfe aktiver Magnetlager. Forschungsberichte Mechatronik & Maschinenakustik. Shaker, Aachen (2009)
18. Lomakin, A.A.: Calculation of critical speed and securing of dynamic stability of hydraulic high-pressure pumps with reference to the forces arising in the gap seals. Energomashinostroenie **4**(1), 1158 (1958)